



HAL
open science

Global significance of oxygen and carbon isotope compositions of pedogenic carbonates since the cretaceous

Marc Jolivet, Philippe Boulvais

► **To cite this version:**

Marc Jolivet, Philippe Boulvais. Global significance of oxygen and carbon isotope compositions of pedogenic carbonates since the cretaceous. *Geoscience Frontiers*, 2021, 12 (4), pp.101132. 10.1016/j.gsf.2020.12.012 . insu-03097898

HAL Id: insu-03097898

<https://insu.hal.science/insu-03097898>

Submitted on 5 Jan 2021

HAL is a multi-disciplinary open access archive for the deposit and dissemination of scientific research documents, whether they are published or not. The documents may come from teaching and research institutions in France or abroad, or from public or private research centers.

L'archive ouverte pluridisciplinaire **HAL**, est destinée au dépôt et à la diffusion de documents scientifiques de niveau recherche, publiés ou non, émanant des établissements d'enseignement et de recherche français ou étrangers, des laboratoires publics ou privés.

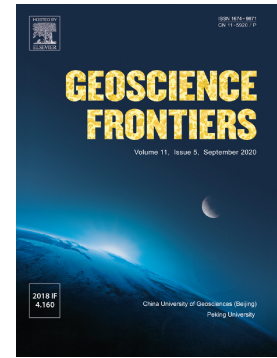


Distributed under a Creative Commons Attribution - NonCommercial - NoDerivatives 4.0 International License

Journal Pre-proof

Global significance of oxygen and carbon isotope compositions of pedogenic carbonates since the cretaceous

Marc Jolivet, Philippe Boulvais



PII: S1674-9871(20)30272-3

DOI: <https://doi.org/10.1016/j.gsf.2020.12.012>

Reference: GSF 1132

To appear in:

Received date: 23 October 2019

Revised date: 24 June 2020

Accepted date: 11 December 2020

Please cite this article as: M. Jolivet and P. Boulvais, Global significance of oxygen and carbon isotope compositions of pedogenic carbonates since the cretaceous, (2020), <https://doi.org/10.1016/j.gsf.2020.12.012>

This is a PDF file of an article that has undergone enhancements after acceptance, such as the addition of a cover page and metadata, and formatting for readability, but it is not yet the definitive version of record. This version will undergo additional copyediting, typesetting and review before it is published in its final form, but we are providing this version to give early visibility of the article. Please note that, during the production process, errors may be discovered which could affect the content, and all legal disclaimers that apply to the journal pertain.

© 2020 Published by Elsevier.

Global significance of oxygen and carbon isotope compositions of pedogenic carbonates since the Cretaceous

Marc Jolivet*, Philippe Boulvais

Géosciences Rennes, CNRS, Univ Rennes, UMR 6118, F-35000 Rennes, France.

*Corresponding Author: marc.jolivet@univ-rennes1.fr

Abstract:

Few global syntheses of oxygen and carbon isotope composition of pedogenic carbonates have been attempted, unlike marine carbonates. Pedogenic carbonates represent *in-situ* indicators of the climate conditions prevailing on land. The $\delta^{18}\text{O}$ and $\delta^{13}\text{C}$ values of pedogenic carbonates are controlled by local and global factors, many of them not affecting the marine carbonates largely used to probe global climate changes. We compile pedogenic oxygen and carbon isotopic data ($N=12167$) from Cretaceous to Quaternary-aged paleosols to identify potential trends through time and tie them to possible controlling factors. While discrete events such as the Paleocene-Eocene Thermal Maximum are clearly evidenced, our analysis reveals an increasing complexity in the distribution of the $\delta^{18}\text{O}$ vs $\delta^{13}\text{C}$ values through the Cenozoic. As could be expected, the rise of C4 plants induces a shift towards higher $\delta^{13}\text{C}$ values during the Neogene and Quaternary. We also show that the increase in global hypsometry during the Neogene plays a major role in controlling the $\delta^{18}\text{O}$ and $\delta^{13}\text{C}$ values of pedogenic carbonates by increasing aridity downwind of orographic barriers. Finally, during the Quaternary, an increase of 3‰ in $\delta^{18}\text{O}$ values is recorded both by the pedogenic carbonates and the marine foraminifera suggesting that both indicators may be used to track global climate signal.

Keywords:

Global isotopic signal; Cretaceous–Quaternary; Pedogenic carbonates; Topography

1 Introduction

The oxygen and carbon isotope compositions of pedogenic carbonates represent archives of past climate and environmental changes (Cerling, 1984, 1991; Fox and Koch, 2004; Dworkin et al., 2005; Garzzone et al., 2008). The $\delta^{18}\text{O}$ and $\delta^{13}\text{C}$ values of pedogenic carbonates are controlled by a number of factors that can be grouped in two broad categories: local factors (evaporation, nature of the vegetation, soil respiration, soil depth, hydrology and elevation of the area, latitude, distance from the marine water source...) and global factors such as atmospheric CO_2 pressure or atmospheric CO_2 isotopic composition (Jenny, 1980; Allison et al., 1984; Cerling, 1991; Körner et al., 1991; Cerling and Quade, 1993). Based on this, paleosol stable isotope data are used to constrain the paleoenvironmental conditions for specific areas and periods of time. More global climate signals are generally probed using the isotopic composition of marine carbonates or of marine and continental fossil records (Zachos et al., 2001; Zeebe, 2001; Puc at et al., 2003; Amiot et al., 2004; Yongdong Wang et al., 2014). These are used as input data in global-scale climate models in order to derive parameters such as atmospheric $p\text{CO}_2$ values, oceanic water temperatures or wind patterns (Licht et al., 2014; Caves et al., 2015; Ladant and Donnadieu, 2016). Whereas long-term, global or at least very large scale trends in isotopic compositions of marine carbonate fossils or continental vertebrates have been described (Puc at et al., 2003; Amiot et al., 2004), only a limited number of global analysis of pedogenic carbonates have been attempted to date (e.g. Ekart et al., 1999; Sheldon and Tabor, 2009), despite these carbonates represent in-situ indicators of the climate conditions prevailing on-land.

A growing dataset of oxygen and carbon isotope compositions is available from carbonate-bearing paleosols worldwide, unevenly covering a long period of time from the Paleozoic to the Quaternary. From this dataset we selected the isotopic values obtained from Cretaceous to Quaternary paleosols. Analyzing those data from a global perspective, over large periods of time, we show that the isotopic signal reflects local and global conditions at a given, relatively short period of time, and that long-term trends in the isotopic data also exist that can be correlated to biological, topographic or climatic conditions.

2 Data collection

In this study we use the data from 103 publications corresponding to geological sites in both hemispheres covering large latitude ranges and distributed on the 5 continents (Fig. 1 and Supplementary Table S1). Only data that were provided as numbers in tables were selected, avoiding collecting data from graphs. In order to get a homogeneous dataset, we selected oxygen and carbon isotope compositions solely from samples that could be assigned with high confidence to pedogenic carbonates (nodules, rhizcretions and pedogenic calcretes), and for which the formation age and the present-day geographic position are indicated. Those samples for which diagenetic alteration has been demonstrated or suspected by the authors of the original publication have been rejected as well as those developed in sediment hosting inherited carbonate grains when this is indicated in the publication. In each individual study, when outliers exist but are not directly explained by factors such as diagenesis, inherited carbonate or potential analytical errors, they have been included in the dataset.

Soil CO₂ is generally a two-components mixture between atmospheric CO₂ and CO₂ derived from *in situ* oxidation of organic carbon (referred as soil respiration). Both soil

pCO₂ and $\delta^{13}\text{C}$ values thus vary with depth from atmospheric values at the surface to a constant soil value at depth, leading to a spread in individual isotopic ratios. Except for very low soil respiration rates, both parameters should be constant below depths of about 50 cm (Cerling, 1984; Sheldon and Tabor, 2009). For studies dealing with Quaternary paleosols and indicating the sampling depth, the values from samples collected above a depth of 50 cm have not been selected. The sampling depth for older paleosols is generally not constrained and all values have been considered. A total number of 12167 data have been isolated. Sheldon (2018) recently proposed to use the difference between the carbon isotope composition of soil carbonate and that of soil organic matter $\Delta^{13}\text{C} = \delta^{13}\text{C}_{\text{carb}} - \delta^{13}\text{C}_{\text{org}}$ to screen corresponding oxygen isotope values and reject those that do not correspond to soils in oxygen isotope equilibrium. However, most of the studies we used in this compilation do not include $\delta^{13}\text{C}_{\text{org}}$ values. To preserve the homogeneity of our dataset we were thus unable to use this approach and did not screen the oxygen isotope values even when $\delta^{13}\text{C}_{\text{org}}$ was available.

The $\delta^{13}\text{C}$ values are given relative to the Pee Dee Belemnite (PDB or VPDB for the equivalent Vienna standard). All $\delta^{18}\text{O}$ values are given relative to the Vienna Standard Mean Ocean Water (VSMOW) and data initially provided using VPDB scale were converted using

$$\delta^{18}\text{O}_{\text{VSMOW}} = 1.03091 \times \delta^{18}\text{O}_{\text{VPDB}} + 30.91 \quad (\text{Coplen et al., 1983})$$

In order to investigate the existence of trends in the data over large time-scales, data have been compiled in five age groups using the ages indicated in the original papers (Fig. 2): Lower Cretaceous, Upper Cretaceous, Paleogene, Neogene and Quaternary. The paleo-location of the samples is reported on the paleogeographic maps of the PALEOMAP project (Scotese, 2014a, b, c, d) (Fig. 1). When not provided in the original

publication, the original paleolatitude of the samples has been estimated using these maps or paleotectonic maps of the Tethyan region (Dercourt et al., 2000; Barrier et al., 2018).

Trends in $\delta^{18}\text{O}$ values through time are also compared to the evolution of global hypsometry notably to assess the role of orographic barriers. The Cretaceous topography was obtained from the 2.8° latitude \times 2.8° longitude paleogeographic reconstructions of Sewall et al. (2007), based on the $1^\circ \times 1^\circ$ paleo Digital Elevation Model (DEM) of the PALEOMAP project (<http://www.scotese.com/Default.htm>, Scotese and Golonka, 1992) modified using data from the literature and from the Deep Time Maps project of R. Blakey (<https://deeptimemaps.com>). The early Eocene paleo DEM is from Herold et al. (2014) and has a $2^\circ \times 2^\circ$ grid resolution. The middle Miocene paleo DEM was taken from Frigola et al. (2018). This model is based on a previous $2^\circ \times 2^\circ$ grid resolution reconstruction by Herold et al. (2008) that the authors modified to take into account recently published paleo-topography information.

Details on the method used to reconstruct each paleo DEM can be found in the corresponding publications and here we only provide a summary of the method. Generally speaking, paleo DEMs are constructed by estimating the topographic resultant of past tectonic settings based on comparison with their modern equivalent (Ziegler et al., 1985). The elevation is defined along contour lines and each grid cell corresponds to a range of elevation and not to a definite value. Each paleo DEM is further corrected using the position of known shorelines or any independent paleo-altitude estimates (paleo-flora, geochemistry, etc.) (Markwick and Valdes, 2004; Markwick, 2007). Finally, a gridded, discrete DEM is obtained through interpolation of the contour lines (Herold et al., 2014). The uncertainty associated to these models are difficult to estimate and vary due to the amount of paleo-elevation data available for each period and to the method

use to integrate those data in the models and interpolate them (Markwick and Valdes, 2004). For example, Herold et al. (2008) published a compilation of paleo-altitude estimates and their uncertainty for the Tibetan plateau and the Andes during the Miocene and Pliocene. Those error margins are generally higher than 500 m and up to 2000 m for the Andes. However, in this study, paleo-elevation data are not used to establish the exact altitude of ranges rather to derive trends in the evolution of the global hypsometry which likely correspond to trends in the complexity of the global topography.

3 Results

3.1. Oxygen

The oxygen isotope composition of paleosols is reported as frequency diagrams along the stratigraphy column (Fig. 2). Diagrams were built using the DensityPlotter program (Vermeesch, 2012) and a Gaussian kernel distribution function. Peaks in the distribution of data are derived from the kernel analysis.

The major peak in the Lower Cretaceous, Upper Cretaceous and Paleogene $\delta^{18}\text{O}$ distributions is near identical centered on $(+22 \pm 0.5)\text{‰}$, although the low number of Lower Cretaceous data makes for less robust statistics. The Cretaceous data possibly display a bimodal distribution with a sub-peak around $+10\text{‰}$ in the Lower Cretaceous and a sub-peak around $+16.7\text{‰}$ in the Upper Cretaceous. Actually, the Lower Cretaceous minor peak corresponds to data obtained from samples collected in southern Australia at a very high paleolatitude of 75°S (Gregory et al., 1989).

The Paleogene distribution contains a minor peak at $(+17.1 \pm 0.5)\text{‰}$ corresponding to a series of samples collected in the Oligocene Upper John Day Formation in Oregon

(Retallack et al., 2004). The authors correlate the low $\delta^{18}\text{O}$ values to cyclic cold periods. Such low values are also reported from the Eocene of Wyoming (USA), and again interpreted as cyclic shifts in seasonal distribution of precipitations inducing increases in soil water content and correlative decrease in $\delta^{18}\text{O}$ values (Clyde et al., 2001). Finally, a few low $\delta^{18}\text{O}$ values are reported from the Eocene of Tibet, interpreted as associated to low temperature, high altitude environments (Hoke et al., 2014b). The proportion of these low $\delta^{18}\text{O}$ values tend to decrease after the Oligocene.

The Neogene distribution of $\delta^{18}\text{O}$ values displays a wide peak, almost a plateau, with a central value of $(+23 \pm 0.5)\text{‰}$. This broad distribution might correspond to a combination between the $(+22 \pm 0.5)\text{‰}$ peak observed in the Cretaceous and Paleogene data and a new population of data with $\delta^{18}\text{O}$ values around $+25\text{‰}$. Very few $\delta^{18}\text{O}$ values are above 30‰ .

A peak at $(+22 \pm 0.5)\text{‰}$ is also observed in the Quaternary distribution; however the main peak corresponds to higher $\delta^{18}\text{O}$ values (at $+25\text{‰}$). This 3‰ difference, which might explain the wide distribution in the Neogene data, also matches the 3‰ increase in the $\delta^{18}\text{O}$ values of deep-sea foraminifera during the same period, generally considered as reflecting the development of polar ice-caps and the cooling of deep-sea waters (Lear et al., 2000; Zachos et al., 2001; Billups and Schrag, 2002) (Fig. 2). A notable feature of the Quaternary dataset is the occurrence of tens of $\delta^{18}\text{O}$ values (above $+30\text{‰}$).

3.2. Carbon

The distribution of the $\delta^{13}\text{C}$ values is largely unimodal from the Cretaceous to the Neogene, although a hint of bimodality occurs in the Lower Cretaceous data (Fig. 2). However, a large number of the high $\delta^{13}\text{C}$ Lower Cretaceous values (up to $+10\text{‰}$) were

mainly obtained from the Otway and Strzelecki ranges in Australia which show a strong data dispersion and should thus be considered with care (Gregory et al., 1989). Unlike in the oxygen data, the major peak of the distribution varies with time, from -6.9‰ in the Lower Cretaceous, decreasing to -9.3‰ and -9.1‰ in the Upper Cretaceous – Paleogene period then increasing to -6.6‰ in the Neogene. The only remarkable exception are the $\delta^{13}\text{C}$ values associated to the Paleocene – Eocene transition Thermal Maximum (PETM) that form a secondary peak around -14‰ in the Paleogene distribution (Bowen et al., 2001; Koch et al., 2003). These low $\delta^{13}\text{C}$ values have been interpreted as resulting from the massive release of carbon from marine methane hydrates during the thermal maximum (Dickens et al., 1997; Bains et al., 1999; Beerling, 2000).

The Quaternary distribution is bimodal with peaks at -6.1‰ and -1.4‰ . An increase in $\delta^{13}\text{C}$ values seems to start in the Neogene distribution. Interestingly, this increase mirrors the decrease of the $\delta^{13}\text{C}$ values of the deep-sea foraminifera observed by Zachos et al. (2001) from the Neogene (Fig. 2).

3.3. $\delta^{13}\text{C}$ vs. $\delta^{18}\text{O}$ values.

Due to the relatively limited number of oxygen and carbon isotope data available for the Cretaceous period, we restricted the visualization of the data in the $\delta^{13}\text{C}$ vs. $\delta^{18}\text{O}$ diagram to the Paleogene – Quaternary time-range (Fig. 3). Data clusters, labelled A to E in Fig. 3, were obtained using a gaussian kernel density function: the occurrence of a cluster is defined by a peak in the density of data. Although the distribution of data within a cluster may not be homogeneous, we considered that the center of the cluster corresponds to the position of the highest density.

Most of the Paleogene data plot within a very narrow range, forming a dense cluster (labelled “A” on Fig. 3). Two smaller clusters (A’ and A’’) are visible, associated to specific time-periods. Cluster A’ with low $\delta^{18}\text{O}$ values but $\delta^{13}\text{C}$ values comparable to cluster A, corresponds to the cyclic colder and/or wetter periods recorded in the USA or Tibet (Clyde et al., 2001; Retallack et al., 2004; Hoke et al., 2014b). Cluster A’’ with low $\delta^{13}\text{C}$ values but $\delta^{18}\text{O}$ values comparable to cluster A corresponds to PETM-related data. Finally, some outliers are distributed into a slightly wider region of the graph with an incipient cluster (B) showing higher $\delta^{18}\text{O}$ values in relation either with evidence of increased aridity or increased hypsometry of the ground-water source region (Clyde et al., 2001; Alonso-Zarza and Arenas, 2004).

The Neogene data form a wide cloud of points with three clusters. Cluster A might correspond to Paleogene cluster A, however slightly shifted towards lower $\delta^{18}\text{O}$ values (by about 1.5‰). Cluster B represents the majority of the data. It displays $\delta^{13}\text{C}$ and $\delta^{18}\text{O}$ central value higher than cluster A. Its position is similar to that of the incipient cluster B observed in the Paleogene data. The third cluster C has $\delta^{13}\text{C}$ values generally higher than those of A and B and $\delta^{18}\text{O}$ values lower than B and similar to slightly higher than A.

The differentiation in several clusters is obvious in the Quaternary data: cluster A defined for Paleogene and Neogene data no longer exists, cluster B becomes major with an increase in the central $\delta^{13}\text{C}$ value and cluster C has largely reduced. Two new clusters (D, E) can be identified, corresponding to an increase in $\delta^{13}\text{C}$ and $\delta^{18}\text{O}$ values, respectively. Also new in the Quaternary data set is the rather high number of samples with both high $\delta^{13}\text{C}$ and $\delta^{18}\text{O}$ values.

4 Discussion

4.1 Global signals: pCO₂, emergence of C4 plants, global cooling and hypsometry

Global, long-term isotopic signals depicted above are registered in carbonate-bearing paleosols implying that global forcing parameters have to be invoked. Some of the Early Cretaceous $\delta^{13}\text{C}$ values (higher than 0‰, Fig. 2, lower right) seem correlated to high pCO₂ values (Lee and Hisada, 1999; Robinson et al., 2002; Huang et al., 2012). Recent multi-proxy compilations have shown that pCO₂ varied largely during the Paleogene. It was variable during the Paleocene with mean values comparable to the present-day ones and much higher during the Eocene with a peak in global warmth during the Ypresian (Beerling and Royer, 2011; Hyland and Sheldon, 2013). These conditions likely explain the spread in $\delta^{13}\text{C}$ values between about -16‰ and 0‰ as the minor peak at -14‰ is clearly related to the PETM.

The pCO₂ being comparatively low during the Neogene, the emergence of high $\delta^{13}\text{C}$ values for that period and the well-defined peak at about -1.4‰ (with data reaching up to about +8‰) for the Quaternary data is largely explained by the Late Miocene rise of C4-dominated ecosystems, with higher- $\delta^{13}\text{C}$ values (Quade and Cerling, 1995; Fox and Koch, 2004; Edwards et al., 2010; Strömberg, 2011). The distribution of the Quaternary $\delta^{13}\text{C}$ data is thus, at first order, dominated by the C3 (major peak in distribution) and C4 (minor peak) plants-dominated environments (Fig. 2). However, unless considering that all the ecosystems that produced the analyzed paleosols contained a significant proportion of C4 plants, this parameter alone does not explain the complete disappearance of cluster (A) in the $\delta^{13}\text{C}$ vs $\delta^{18}\text{O}$ plot (Fig. 3).

Besides the emergence of C4 plants, two other main events distinguish the late Paleogene – Quaternary period from the Cretaceous – Early Paleogene that likely influence the isotopic signals. These are (1) the middle Eocene – Oligocene development

of the Antarctic Ice cap and of more ephemeral ice in the Arctic (Tripathi and Darby, 2018), followed by the late Miocene – Pliocene extension of Arctic glaciation (Larsen et al., 1994; Helland and Holmes, 1997), and (2) the Oligocene – Miocene rise of several large mountain ranges. These reliefs increased the number and size of orographic barriers, disrupting the atmospheric circulation.

The Neogene – Quaternary period is marked by a general increase of the $\delta^{18}\text{O}$ values of pedogenic carbonates (Fig. 2). In the oceanic realm, the Oligocene and Late Miocene – Quaternary global cooling phases induced a comparable increase in the $\delta^{18}\text{O}$ value of deep-sea foraminifera (Fig. 2; Zachos et al., 2001). Unless considering that, during the Late Miocene – Quaternary period, the global ocean was isotopically unbalanced due to a large amount of low $\delta^{18}\text{O}$ water stored in the polar ice-caps and permafrost soils, cooler global temperatures should lead to lower $\delta^{18}\text{O}$ rainfall values and therefore to lower $\delta^{18}\text{O}$ values in paleosol carbonates. For example, this temperature effect is put forward to explain the low $\delta^{18}\text{O}$ values registered in the Early Cretaceous, high-latitude paleosols of southern Australia (Gregory et al., 1989) (Fig. 2). However, cooler temperatures should also increase the CaCO_3 – H_2O fractionation factor, leading to an increase in the $\delta^{18}\text{O}$ values of paleosol carbonates (Cerling, 1984). This effect might participate to the increase of $\delta^{18}\text{O}$ values during the Neogene and Quaternary (Figs. 2 and 3).

Although some mountain ranges such as the North American Cordillera existed during the Cretaceous (Wernicke et al., 1987; Yonkee and Weil, 2015), global hypsometry increased during the Neogene with the formation or enhanced uplift of mountain ranges such as the Andes (Hoke and Garziona, 2008), the increased uplift and spreading of the Tibetan plateau (Tapponnier et al., 2001; Kirby et al., 2002; Liu-Zeng et al., 2008; Cheng et al., 2016), the topographic growth of the Tian Shan, Altai and Sayan ranges in central

Asia (Jolivet et al., 2010, 2013, 2018a), the rise of the Alps (Schmid et al., 1996; Willett et al., 2006; Labaume et al., 2008) or the formation of the Southern Alps (Tippett and Kamp, 1995; Chamberlain et al., 1999)(Fig. 4). These new reliefs increased the number and size of orographic barriers, disrupting the atmospheric circulation and leading to the development of monsoon-type climates and the formation of rain shadows (Broccoli and Manabe, 1992; Dettman et al., 2003; Harris, 2006; Caves et al., 2014). Although the exact relation between the Himalayan monsoon and the aridification of Central Asia remains debated (e.g. Licht et al., 2014), it has, for example, been recently shown that loess deposits started to form during the latest Eocene in the central part of the Rocky Mountains (North America) in response to enhanced uplift of the range. Aridification was further increased by the global climate cooling at the Eocene–Oligocene Transition but its onset seems indeed related to orographic processes (Fan et al., 2020). Central Asia provides a good example of the isotropic effect of relief building. In that region, two phenomena are acting to increase the $\delta^{18}\text{O}$ values of paleosol carbonates: the low- $\delta^{18}\text{O}$ moisture evaporated from the Indian Ocean to the south is blocked by the Himalayas and rainfalls are mainly sourced from high- $\delta^{18}\text{O}$ moisture transported by the Westerlies (Bershaw et al., 2012; Caves et al., 2015); in parallel, aridity increased during the Late Paleogene – Quaternary period (Bosboom et al., 2014), which led to stronger evaporation and to an increase in $\delta^{18}\text{O}$ values of soil water.

We thus suggest that the global increase in hypsometry during the Late Paleogene – Quaternary period, leading to enhanced regional aridification due to rain shadow effects is registered as a first order signal in the evolution of the isotopic composition of carbonate paleosols. The parallel shift towards higher $\delta^{18}\text{O}$ values in deep-sea foraminifera and pedogenic carbonates during the Quaternary remains to be explored further. We acknowledge that the parallel deviation of both dataset could be fortuitous

but cannot ignore the possibility that, at least for the Quaternary period, both signals record modification in oceanic water oxygen isotopic ratio.

4.2 Some examples of second order trends

Second order signals, limited to a specific period of time and/or to a specific locality can also be derived from the present global survey. Some of these are illustrated below despite not being always completely understood.

The first order influence of topography and associated enhanced aridity can be blurred by local effects. A first group of parameters tends to decrease the $\delta^{18}\text{O}$ values such as the decrease in $\delta^{18}\text{O}$ values of rainfall with altitude (Poage and Chamberlain, 2001), the mixing between rainfall water and river water coming from high altitude orographic rainfalls (Charreau et al., 2012; Jolivet et al., 2018b) or the development of large fresh-water lakes (Jolivet et al., 2018b). On the other hand, increasing evaporation tends to increase the oxygen isotopic composition towards higher values. In some hyper-arid regions such as the Atacama desert, the effects of extreme evaporation makes for carbonates $\delta^{18}\text{O}$ values incompatible with those expected from carbonates formed in isotopic equilibrium with rainfall water (Quade et al., 2007). In the same regions, rapid evaporation of rain water implies that carbonates form close or at the surface, in isotopic equilibrium with the atmospheric CO_2 and not with the soil CO_2 (Quade et al., 2007). This hyper-aridity likely explains the position of the Quaternary samples having both the highest $\delta^{18}\text{O}$ and $\delta^{13}\text{C}$ values in Fig. 3. Similarly, in C3 dominated ecosystems, the $\delta^{13}\text{C}$ value of paleosol carbonates increases with increasing hydric stress (and the coeval decrease in soil respiration capacities) (Kohn, 2010). These secondary parameters likely explain part of the spread in $\delta^{18}\text{O}$ and $\delta^{13}\text{C}$ values observed for the Neogene and Quaternary periods (Fig. 2).

As expected from theoretical models (e.g. Cerling and Quade, 1993), the Quaternary mean $\delta^{18}\text{O}$ value of each individual dataset shows a weak negative correlation with absolute latitude within the documented range of 4° – 45° (Fig. 5a). Between 25° and 40° the large spread in the data is probably related to local variations in evaporation and rainfall following the topographic factors described above. However, the theoretical relationship between the $\delta^{18}\text{O}$ values and latitude is only observed in the Quaternary dataset, not for the other periods. The Quaternary mean $\delta^{13}\text{C}$ values show a positive correlation with latitude between 4° and 30° possibly linked to the increase in aridity and relative proportion of C_3 and C_4 plants in the ecosystems (Fig. 5b). Actually, altitude, by influencing the local climate (especially the mean temperature of the warmest months), also plays a role in the competition between C_4 and C_3 plants (Cotton et al., 2014; Hyland et al., 2019). Above 30° latitude, the mean $\delta^{13}\text{C}$ values in the Quaternary datasets are largely spread, again probably in response to the impact of complex topography on the ecosystems and soil conditions.

Correlations, positive or negative, exist in the $\delta^{13}\text{C}$ vs. $\delta^{18}\text{O}$ plot of individual datasets (Fig. 6a, b). Positive correlations are well documented in the Quaternary and to a lesser extent in the Neogene dataset (see for example the data of Salomons et al. (1978); Cerling and Hay (1985) or Potts et al. (2009) for the Quaternary and Latorre et al. (1997) for the Neogene). These trends covering time span of several 10 kyrs to several Myrs are usually explained by climate and ecosystem changes through time: an increase in aridity leads to increased evaporation (inducing higher $\delta^{18}\text{O}$ values), soil hydric stress (inducing higher $\delta^{13}\text{C}$ values) and favors C_4 plants (again increasing the $\delta^{13}\text{C}$ values). Negative correlations are observed in the Quaternary (Yang Wang and Shu-Hui Zheng, 1989), possibly in the Neogene (Charreau et al., 2012) and to a larger extend in the Paleogene (Koch et al., 1995; Alonso-Zarza and Arenas, 2004) (Fig. 6c–e). Few authors

discussed such negative correlations that remain poorly explored. Only (Alonso-Zarza and Arenas, 2004) proposed that it could be controlled by climate: the driest periods would also be cooler, leading to high $\delta^{13}\text{C}$ values, associated to a limited variation in $\delta^{18}\text{O}$ compared to wetter, warmer periods. Finally, some of the Quaternary (Alam et al., 1997; Alomar, 2001) and Neogene datasets (Behrensmeyer et al., 2007) show a wide range in $\delta^{13}\text{C}$ values associated to a narrow $\delta^{18}\text{O}$ range (Fig. 6f, g). Most authors explain the large spread in $\delta^{13}\text{C}$ values by changes in the proportion of C3 over C4 plants, associated to small variations in climate conditions. However, Alomar (2001) suggested that changes in $\delta^{13}\text{C}$ values could also result from fluctuations in the atmospheric component of soil CO_2 .

5 Conclusions

The analysis presented here is based on the oxygen and carbon isotope data of pedogenic carbonates of the Cretaceous up to the Quaternary. We show that pedogenic carbonates record long-term, global isotopic signals, complementary to the record of oceanic carbonates. For example, whereas the influence of polar ice-caps from the Late Paleogene (and possibly during the Upper Cretaceous) is recorded in the oceanic $\delta^{18}\text{O}$ signal, the effects of global continental hypsometry are not. In that respect, continental topography and associated enhanced aridity became a major forcing parameter during the Neogene and Quaternary periods, creating regional- to local-scale climatic conditions leading in turn to contrasted ecosystems. This complex climatic and biologic pattern, associated to the rise of C4 plants during the Neogene, seems to have led to uniquely complex soil carbonates $\delta^{18}\text{O}$ and $\delta^{13}\text{C}$ patterns.

Acknowledgements

We would like to thank Ch. Lecuyer for helpful discussions, A. Kaakinen and J. Andrews for providing access to datasets and two reviewers for their very helpful comments and suggestions. Funding for authors salaries was from Centre National de la Recherche Scientifique for M. Jolivet and University Rennes 1 for Ph. Boulvais.

Data Availability Statement

Data sharing is not applicable to this article as no new data were created or analyzed in this study.

References:

- Achyuthan, H., 2003. Petrologic analysis and geochemistry of the Late Neogene – Early Quaternary hardpan calcretes of Western Rajasthan, India. *Quat. Int.* 106-107, 3-10.
- Achyuthan, H., Shankar, N., Braida, M., Ahmad, S.M., 2012. Geochemistry of calcretes (caliche palaeosols and hardpan), Coimbatore, Southern India: Formation and paleoenvironment. *Quat. Int.* 263, 155-169.
- Alam, M.S., Keppens, E., Paepe, F., 1997. The use of oxygen and carbon isotope composition of pedogenic carbonates from Pleistocene palaeosols in NW Bangladesh, as palaeoclimatic indicators. *Quat. Sci. Rev.* 16, 161-168.
- Allison, G.B., Barnes, C.J., Hughes, M.W., Leary, F.W.J., 1984. The effect of climate and vegetation on the oxygen-18 and deuterium profiles in soils. *Isotope Hydrology 1983*. In: *Proceedings of the Symposium IAEA, Vienna, Austria*, pp. 105-123.
- Alomar, L., 2001. Stable isotope geochemistry of caliche in the Blackwater Draw Formation, Southern High Plains, Texas. M.S. Thesis, Texas Tech University, 69 p.
- Alonso-Zarza, A.M., Arenas, C., 2004. Cenozoic calcretes from the Teruel graben, Spain: microstructure, stable isotope geochemistry and environmental significance. *Sediment. Geol.* 167, 91-108.

- Amiot, R., Lécuyer, Ch., Buffetaut, E., Fluteau, F., Legendre, S., Martineau, F., 2004. Latitudinal temperature gradient during the Cretaceous Upper Campanian-Middle Maastrichtian: $d^{18}O$ record of continental vertebrates. *Earth Planet. Sci. Lett.* 226, 255-271.
- Andrews, J.E., Singhvi, A.K., Kailath, A.J., Kuhn, R., Dennis, P.F., Tandon, S.K., Dhir, R.P., 1998. Do stable isotope data from calcrete record Late Pleistocene monsoonal climate variation in the Thar desert of India? *Quat. Res.* 50, 240-251.
- Aronson, J.L., Hailemichael, M., Savin, S.M., 2008. Hominid environments at Hadar from paleosol studies in a framework of Ethiopian climate change. *J. Hum. Evol.* 55, 532-550.
- Bains, S., Corfield, R.M., Norris, R.D., 1999. Mechanisms of climate warming at the end of the Paleocene. *Science* 285, 724-727.
- Barrier, E., Vrielynck, B., Brouillet, J.-F., Brunet, M.-F., 2018. Paleotectonic Reconstruction of the Central Tethyan Realm. *Tectono-Sedimentary-Palinspastic maps from Late Permian to Pliocene*. CGMW, Paris.
- Beerling, D.J., 2000. Increased terrestrial carbon storage across the Palaeocene-Eocene boundary. *Paleogeogr. Paleoclimatol. Paleoecol.* 161, 395-405.
- Beerling, D.J., Royer, D.L., 2011. Convergent Cenozoic CO_2 history. *Nat. Geosci.* 4, 418-420.
- Behrensmeyer, A.K., Quade, J., Cerling, T.E., Kappelman, J., Khan, I.A., Copeland, P., Roe, L., Hicks, J., Stubblefield, P., Willis, B.J., Latorre, C., 2007. The structure and rate of late Miocene expansion of C_4 plants: Evidence from lateral variation in stable isotopes in paleosols of the Siwalik Group, northern Pakistan. *Geol. Soc. Am. Bull.* 119, 1486-1505.
- Bershaw, J., Garzzone, C.N., Schoenbohm, L., Gehrels, G., Tao, L., 2012. Cenozoic evolution of the Pamir plateau based on stratigraphy, zircon provenance, and stable isotopes of

- foreland basin sediments at Oytug (Wuyitake) in the Tarim Basin (West China). *J. Asian Earth Sci.* 44, 136-148.
- Billups, K., Schrag, D.P., 2003. Application of benthic foraminiferal Mg/Ca ratios to questions of Cenozoic climate change. *Earth Planet. Sci. Lett.* 209, 181-195.
- Bojar, A.V., Csiki, Z., Grigorescu, D., 2010. Stable isotope distribution in Maastrichtian vertebrates and paleosols from the Hateg Basin, South Carpathians. *Paleogeogr. Paleoclimatol. Paleoecol.* 293, 329-342.
- Bosboom, R., Abels, H.A., Hoorn, C., van den Berg, B.C.J., Guo, Z., Dupont-Nivet, G., 2014. Aridification in continental Asia after the Middle Eocene Climatic Optimum (MECO). *Earth Planet. Sci. Lett.* 389, 34-42.
- Boucot, A.J., Scotese, C.R., Chen, X., Morley, R.J., 2013. Phanerozoic paleoclimate: An Atlas of lithologic indicators of climate. In: Nichols, G.J., Ricketts, B. (Eds.), *Concept in Sedimentology and Paleontology*. Society for Sedimentary Geology, Tulsa, 1-478 p.
- Bowen, G.J., Koch, P.L., Gingerich, P.D., Norris, R.D., Bains, S., Corfield, R.M., 2001. Refined isotope stratigraphy across the continental Paleocene-Eocene boundary on Polecat Bench in the northern Bighorn Basin. In: Gingerich, P.D. (Ed.), *Paleocene-Eocene Stratigraphy and Biotic Change in the Bighorn and Clarks Fork Basins, Wyoming*. University of Michigan Papers on Paleontology, 33, 73-88.
- Bowen, G.J., Koch, P.L., Meng, J., Ye, J., Ting, S., 2005. Age and correlation of fossiliferous Late Paleocene-Early Eocene strata of the Erlan Basin, Inner Mongolia, China. *Am. Mus. Novit.* 3474, 1-26.
- Brek, M., Glumac, B., 2014. Stable isotopic ($\delta^{13}\text{C}$ and $\delta^{18}\text{O}$) signatures of biogenic calcretes marking discontinuity surfaces: a case study from Upper Cretaceous carbonates of central Dalmatia and eastern Istria, Croatia. *Facies* 30, 773-788.

- Broccoli, A.J., Manabe, S., 1992. The effects of orography on midlatitude northern hemisphere dry climates. *J. Clim.* 5, 1181-1201.
- Caves, J.K., Sjostrom, D.J., Mix, H.T., Winnick, M.J., Chamberlain, C.P., 2014. Aridification of Central Asia and uplift of the Altai and Hangay Mountains, Mongolia: Stable isotope evidence. *American Journal of Sciences* 314, 1171-1201.
- Caves, J.K., Winnick, M.J., Graham, S.A., Sjostrom, D.J., Mulch, A., Chamberlain, C.P., 2015. Role of the westerlies in Central Asia climate over the Cenozoic. *Earth Planet. Sci. Lett.* 428, 33-43.
- Caves, J.K., Bayshashov, B.U., Zhamangara, A., Ritch, A.J., Pliamra, D.E., Sjostrom, D.J., Mix, H.T., Winnick, M.J., Chamberlain, C.P., 2017. Late Miocene uplift of the Tian Shan and Altai and reorganization of Central Asia climate. *GSA Today* 27(2), 19-26. doi: 10.1130/GSATG305A.1.
- Cerling, T.E., 1984. The stable isotopic composition of modern soil carbonate and its relationship to climate. *Earth Planet. Sci. Lett.* 71, 229-240.
- Cerling, T.E., 1991. Carbon dioxide in the atmosphere: evidence from Cenozoic and Mesozoic paleosols. *American Journal of Science* 291, 377-400.
- Cerling, T.E., 1992. Use of carbon isotopes in paleosols as an indicator of the $P(\text{CO}_2)$ of the paleoatmosphere. *Glob. Biogeochem. Cycle* 6(3), 307-314.
- Cerling, T.E., Bowman, J.R., O'Neil, J.R., 1988. An isotopic study of a fluvial-lacustrine sequence: the Plio-Pleistocene Koobi Fora sequence, East Africa. *Paleogeogr. Paleoclimatol. Paleoecol.* 63, 335-356.
- Cerling, T.E., Hay, R.L., 1986. An isotopic study of paleosol carbonates from Olduvai gorge. *Quat. Res.* 25, 63-78.

- Cerling, T.E., Wynn, J.G., Andanje, S.A., Bird, M.I., Kimutai Korir, D., Levin, N.E., Mace, W., Macharia, A.N., Quade, J., Remien, C.H., 2011. Woody cover and hominid environments in the past 6 million years. *Nature* 476, 51-56.
- Cerling, T.E., Quade, J., Ambrose, S.H., Sikes, N.E., 1991. Fossil soils, grasses, and carbon isotopes from Fort Ternan, Kenya: grassland or woodland? *J. Hum. Evol.* 21, 295-306.
- Cerling, T.E., Quade, J., 1993. Stable carbon and oxygen isotopes in soil carbonates. *Climate Change in Continental Isotopic Records. American Geophysical Union Geophysical Monograph* 78, 217-231.
- Chamberlain, C.P., Poage, M.A., Craw, D., Reynolds, R.C., 1999. Topographic development of the Southern Alps recorded by the isotopic composition of authigenic clay minerals, South Island, New Zealand. *Chem. Geol.* 155, 279-294.
- Charreau, J., Kent-Corson, M.L., Barrier, L., Angier, R., Ritts, B.D., Chen, Y., France-Lannord, Ch., Guilmette, C., 2012. A high-resolution stable isotopic record from the Junggar Basin (NW China): Implications for the paleotopographic evolution of the Tianshan Mountains. *Earth Planet. Sci. Lett.* 341-344, 158-169.
- Cheng, F., Fu, S.T., Jolivet, M., Zhang, C.H., Guo, Z.J., 2016. Source to sink relation between the eastern Kunlun Range and the Qaidam Basin, northern Tibetan Plateau, during the Cenozoic. *Geol. Soc. Am. Bull.* 128(1-2), 258-283. doi:10.1130/B31260.1
- Clyde, W.C., Sheldon, N.D., Koch, P.L., Gunnell, G.F., Bartels, W.S., 2001. Lining Wasatchian/Bridgerian boundary to the Cenozoic Global Climate Optimum: new magnetostratigraphic and isotopic results from South Pass, Wyoming. *Paleogeogr. Paleoclimatol. Paleoecol.* 167, 175-199.
- Coplen, T.B., Kendall, C., Hopple, J., 1983. Comparison of stable isotope reference samples. *Nature* 302, 236-238.

- Cotton, J.M., Hyland, E.G., Sheldon, N.D., 2014. Multi-proxy evidence for tectonic control on the expansion of C₄ grasses in northwest Argentina. *Earth Planet. Sci. Lett.* 395, 41-50.
- Cramer, B.S., Miller, K.G., Barrett, P.J., Wright, J.D., 2011. Late Cretaceous–Neogene trends in deep ocean temperature and continental ice volume: Reconciling records of benthic foraminiferal geochemistry ($\delta^{18}\text{O}$ and Mg/Ca) with sea level history. *J. Geophys. Res.-Oceans* 116, C12023.
- Dar, R.A., Chandra, R., Romshoo, S.A., Lone, M.A., Ahmad, S.M., 2015. Isotopic and micromorphological studies of Late Quaternary loess-paleosol sequences of the Karewa Group: Inferences for paleoclimate of Kashmir Valley. *Quat. Int.* 265, 155-169.
- De Pelsmaeker, E., Jolivet, M., Dransart Laborde, A., Poujol, M., Robin, C., Zhimulev, F.I., Nachtergaele, S., Glorie, S., De Clercq, S., Kataliev, V.Y., De Grave, J., 2018. Source-to-sink relations in the Kyrgyz Tien Shan from the Jurassic to the Paleogene: insights from sedimentological and detrital zircon U-Pb analyses. *Gondwana Res.* 54, 180-204.
- Dercourt, J., Guetani, M., Vrielynck, B., 2000. Atlas Peri-Téthys and explaining notes (Coord. S. Crasquin). CCGM, Paris, 268p.
- Dettman, D.L., Fang, X.M., Garzzone, C.N., Li, J.J., 2003. Uplift-driven climate change at 12 Ma: a long $\delta^{18}\text{O}$ record from the NE margin of the Tibetan plateau. *Earth Planet. Sci. Lett.* 214, 267-277.
- Deutz, P., Montañez, I.P., Monger, H.C., Morrison, J., 2001. Morphology and isotope heterogeneity of Late Quaternary pedogenic carbonates: Implications for paleosol carbonates as paleoenvironmental proxies. *Paleogeogr. Paleoclimatol. Paleoecol.* 166, 293-317.
- Dhir, R.P., Singhvi, A.K., Andrews, J.E., Kar, A., Sareen, B.K., Tandon, S.K., Kailath, A., Thomas, J.V., 2010. Multiple episodes of aggradation and calcrete formation in Late Quaternary aeolian sands, Central Thar desert, Rajasthan, India. *J. Asian Earth Sci.* 37, 10-16.

- Dickens, G.R., Castillo, M.M., Walker, J.C.G., 1997. A blast of gas in the latest Paleocene: Simulating first-order effects of massive dissociation of oceanic methane hydrate. *Geology* 25, 259-262.
- Dworkin, S.L., Nordt, L., Atchley, S., 2005. Determining terrestrial paleotemperatures using the oxygen isotopic composition of pedogenic carbonate. *Earth Planet. Sci. Lett.* 237, 56-68.
- Edwards, E.J., Osborne, C.P., Strömberg, C.A.E., Smith, S.A., C₄ Grasses Consortium, 2010. The origin of C₄ grasslands: Integrating evolutionary and ecosystem science. *Science* 328, 587-591.
- Eren, E., 2011. Stable isotope geochemistry of Quaternary calcretes in the Mersin area, southern Turkey – A comparison and implications for their origin. *Chemie der Erde* 71, 31-37.
- Fan, M.J., Feng, R., Geissman, J.W., Poulson, C.J., 2020. Late Paleogene emergence of a North American loess plateau. *Geology* 48, 273-277.
- Fox, D.L., Koch, P.L., 2004. Carbon and oxygen isotopic variability in Neogene paleosol carbonates: constraints on the evolution of the C₄-grasslands of the Great Plains, USA. *Paleogeogr. Paleoclimatol. Paleoecol.* 207, 305-329.
- Fox, D.L., Honey, J.G., Martin, R.A., Peláez-Campomanes, P., 2012. Pedogenic carbonate stable isotope record of environmental change during the Neogene in the southern Great Plains, southwest Kansas, USA: Oxygen isotopes and paleoclimate during the evolution of C₄-dominated grassland. *Geol. Soc. Am. Bull.* 124, 431-443.
- Frigola, A., Prange, M., Schulz, M., 2018. Boundary conditions for the Middle Miocene Climate Transition (MMCT v1.0). *Geoscience Model Development* 11, 1607-1626.

- Gao, Y., Ibarra, C.E., Wang, C., Caves, J.K., Chamberlain, C.P., Graham, S.A., Wu, H., 2015. Mid-latitude terrestrial climate of East Asia linked to global climate in the Late Cretaceous. *Geology* 43, 287-290.
- Garrett, N.D., Fox, D.L., McNulty, K.P., Faith, J.T., Peppe, D.J., Van Plantinga, A., Tryon, C.A., 2015. Stable isotope paleoecology of Late Pleistocene Middle Stone Age humans from the Lake Victoria basin, Kenya. *J. Hum. Evol.* 82, 1-14.
- Garzzone, C.N., Hoke, G.D., Libarkin, J.C., Withers, S., MacFadden, B., Eiler, J., Ghosh, P., Mulch, A., 2008. Rise of the Andes. *Science* 230, 1304-1307.
- Ghosh, P., Bhattacharya, S.K., Jani, R.A., 1995. Palaeoclimate and palaeovegetation in central India during the Upper Cretaceous based on stable isotope composition of the palaeosol carbonates. *Paleogeogr. Paleoclimatol. Paleoecol.* 114, 285-296.
- Ghosh, P., Garzzone, C.N., Eiler, J.M., 2006. Rapid uplift of the Altiplano revealed through ^{13}C - ^{18}O bonds in paleosol carbonates. *Science* 311, 511-515.
- Giambiagi, L.B., 1999. Los depositos Neogenos de la region del Rio Palomares, Cordillera Principal de Mendoza. *Revista de la Asociación Geología Argentina* 54, 47-59.
- Gregory, R.T., Douthitt, C.B., Duddy, I.R., Rich, P.V., Rich, T.H., 1989. Oxygen isotopic composition of carbonate concretions from the lower Cretaceous of Victoria, Australia: implications for the evolution of meteoric waters on the Australian continent in a paleopolar environment. *Earth Planet. Sci. Lett.* 92, 27-42.
- Harris, N., 2006. The elevation history of the Tibetan Plateau and its implications for the Asian monsoon. *Paleogeogr. Paleoclimatol. Paleoecol.* 241, 4-15.
- Heilbronn, G., Boulvais, P., Marchand, E., Robin, C., Bourquin, S., Barrier, L., Jia, Y., Fu, B., Jolivet, M., 2015. Stable isotope characterization of pedogenic and lacustrine carbonates from the Chinese Tian Shan: Constraints on the Mesozoic-Lower Cenozoic palaeoenvironmental evolution. *Chemie der Erde* 75, 133-141.

- Helland, P.E., Holmes, M.A., 1997. Surface textural analysis of quartz sand grains from ODP Site 918 off the southeast coast of Greenland suggests glaciation of southern Greenland at 11 Ma. *Paleogeogr. Paleoclimatol. Paleoecol.* 135, 109–121.
- Hellwig, A., Voigt, S., Mulch, A., Frisch, K., Bartenstein, A., Pross, J., Gerdes, A., Voigt, T., 2018. Late Oligocene to early Miocene humidity change recorded in terrestrial sequences in the Ili Basin (south-eastern Kazakhstan, Central Asia). *Sedimentology* 65, 517-539.
- Herold, N., Seton, M., Müller, R.D., 2008. Middle Miocene tectonic boundary conditions for use in climate models. *Geochem. Geophys. Geosyst.* 9, Q10009. doi:10.1029/2008GC002046.
- Herold, N., Buzan, J., Seton, M., Goldner, A., Green, J.A.M., Müller, R.D., Markwick, P., Huber, M., 2014. A suite of early Eocene (~55 Ma) climate model boundary conditions. *Geoscience Model Development* 7, 2077-2091.
- Hoke, G.D., Garzione, C.N., 2008. Paleosurfaces, paleoelevation, and the mechanisms for the late Miocene topographic development of the Altiplano plateau. *Earth Planet. Sci. Lett.* 271, 192-201.
- Hoke, G.D., Liu-Zeng, J., Hren, M.T., Wissink, G.K., Garzione, C.N., 2014a. Stable isotopes reveal high southern Tibetan Plateau margin since the Paleogene. *Earth Planet. Sci. Lett.* 394, 270-278.
- Hoke, G.D., Giambiagi, L.B., Garzione, C.N., Mahoney, J.B., Strecker, M.R., 2014b. Neogene paleoelevation of intermontane basins in a narrow, compressional mountain range, southern Central Andes of Argentina. *Earth Planet. Sci. Lett.* 406, 153-164.
- Huang, C.M., Retallack, G.J., Wang, C.S., 2012. Early Cretaceous atmospheric pCO₂ levels recorded from pedogenic carbonates in China. *Cretac. Res.* 33, 42-49.

- Huerta, P., Armenteros, I., 2005. Calcrete and palustrine assemblages on a distal alluvial-floodplain: A response to local subsidence (Miocene of the Duero basin, Spain). *Sediment. Geol.* 177, 253-270.
- Hyland, E., Sheldon, N.D., 2013. Coupled CO₂-climate response during the early Eocene climatic optimum. *Paleogeogr. Paleoclimatol. Paleoecol.* 369, 125-135.
- Hyland, E.G., Sheldon, N.D., Smith, S.Y., Strömberg, C.A.E., 2019. Late Miocene rise and fall of C₄ grasses in the western United States linked to aridification and uplift. *Geol. Soc. Am. Bull.* 131(1/2), 224-234.
- Irigoyen, M.V., Buchan, K.L., Brown, R.L., 2000. Magnetostereography of Neogene Andean foreland-basin strata, lat 33°S, Mendoza Province, Argentina. *Geol. Soc. Am. Bull.* 112, 803-816.
- Jenny, H., 1980. *The Soil Resource: Origin and Behavior*. Springer Verlag, Berlin.
- Jolivet, M., Dominguez, S., Charreau, J., Chen, Y., Li, Y.A., Wang, Q.C., 2010. Mesozoic and Cenozoic tectonic history of the Central Chinese Tian Shan: Reactivated tectonic structures and active deformation. *Tectonics* 29, TC6019. doi:10.1029/2010TC002712.
- Jolivet, M., Arzhannikov, S., Arzhannikova, A., Chauvet, A., Vassallo, R., Braucher, R., 2013. Geomorphic Mesozoic and Cenozoic evolution in the Oka-Jombolok region (East Sayan ranges, Siberia). *J. Asian Earth Sci.* 62, 117-133.
- Jolivet, M., Barrier, L., Dauteuil, O., Laborde, A., Li, Q., Reichenbacher, B., Popescu, S.-M., Sha, J.G., Guo, Z.J., 2018a. Late Cretaceous-Palaeogene topography of the Chinese Tian Shan: New insights from geomorphology and sedimentology. *Earth Planet. Sci. Lett.* 499, 95-106.

- Jolivet, M., Boulvais, Ph., Barrier, L., Robin, C., Heilbronn, G., Ledoyen, J., Ventroux, Q., Jia, Y., Guo, Zh., Bataleva, E.A., 2018b. Oxygen and carbon stable isotope composition of Cretaceous to Pliocene calcareous paleosols in the Tian Shan region (Central Asia): controlling factors and paleogeographic implications. *Geosciences* 8, 330. doi:10.3390/geosciences80900330.
- Jordan, T., Tamm, V., Figueroa, G., Flemings, P.B., Richards, D., Tabbutt, K., Cheatham, T., 1996. Development of the Miocene Manantiales foreland basin, Principal Cordillera, San Juan, Argentina. *Revista Geológica de Chile* 23, 43-79.
- Kaakinen, A., Sonninen, E., Lunkka, J.P., 2006. Stable isotope record in paleosol carbonates from the Chinese Loess Plateau: Implications for late Neogene paleoclimate and paleovegetation. *Paleogeogr. Paleoclimatol. Paleoecol.* 237, 359-369.
- Kaplan, M.Y., Eren, E., Kadir, S., Kapur, S., 2014. Mineralogical, geochemical and isotopic characteristics of Quaternary calcretes in the Adana region, southern Turkey: Implications on their origin. *Catena* 101, 164-177.
- Kingston, J.D., 1992. Stable isotopic evidence for hominid paleoenvironments in East Africa. Ph.D. thesis, Harvard University, Cambridge, Massachusetts, USA.
- Kleinert, K., Strecker, M.P., 2001. Climate change in response to orographic barrier uplift: Paleosol and stable isotope evidence from the late Neogene Santa María basin, northwestern Argentina. *Geol. Soc. Am. Bull.* 113, 728-742.
- Kirby, E.P.W., Reiners, M.A., Krol, K.X., Whipple, K.V., Hodges, K.A., Farley, W., Tang, Z., Chen, Z., 2002. Late Cenozoic evolution of the eastern margin of the Tibetan Plateau: inferences from $^{40}\text{Ar}/^{39}\text{Ar}$ and (U-Th)/He thermochronology. *Tectonics* 21, 1-20.
- Koch, P.L., Zachos, J.C., Dettman, D.L., 1995. Stable isotope stratigraphy and paleoclimatology of the Paleogene Bighorn Basin (Wyoming, USA). *Paleogeogr. Paleoclimatol. Paleoecol.* 115, 61-89.

- Koch, P.L., Clyde, W.C., Hepple, R.P., Fogel, M.L., Wing, S.L., Zachos, J.C., 2003. Carbon and oxygen isotope records from paleosols spanning the Paleocene-Eocene boundary, Bighorn Basin, Wyoming. In: Wing, S.L., Gingerich, P.D., Schmitz, B., Thomas, E. (Eds.), *Cause and Consequences of Globally Warm Climates in the Early Paleogene*. Geological Society of America, Special Paper, 369, 49-64.
- Kohn, M.J., 2010. Carbon isotope compositions of terrestrial C3 plants as indicators of (paleo)ecology and (paleo)climate. *Proceedings of the National Academy of Sciences, America*, 107, 19691-19695.
- Körner, C., Farquhar, G., Wong, S.C., 1991. Carbon isotope discrimination by plants follows latitudinal and altitudinal trends. *Oecologia* 88, 30-40.
- Kottek, M., Grieser, J., Beck, C., Rudolf, B., Rubel, F., 2006. World map of the Köppen-Geiger climate classification updated. *Meteorologische Zeitschrift* 15, 259-263.
- Labauve, P., Jolivet, M., Souquière, F., Caravet, A., 2008. Tectonic control on diagenesis in a foreland basin: combined petrologic and thermochronologic approaches in the Grès d'Annot basin (Late Eocene – Early Oligocene, French-Italian external Alps). *Terra Nova* 20, 95-101.
- Ladant, J.B., Donnadieu, Y., 2016. Palaeogeographic regulation of glacial events during the Cretaceous supergreenhouse. *Nature Communications* 7, 12771. DOI: 10.1038/ncomms12771.
- Larsen, H.C., Saunders, A.D., Clift, P.D., Beget, J., Wei, W., Spezzaferri, S., 1994. ODP Leg 152 Scientific Party, Seven million years of glaciation in Greenland. *Science* 264, 952-956.
- Latorre, C., Quade, J., McIntosh, W.C., 1997. The expansion of C₄ grasses and global change in the late Miocene: Stable isotope evidence from the Americas. *Earth Planet. Sci. Lett.* 146, 83-96.

- Lear, C.H., Elderfield, H., Wilson, P.A., 2000. Cenozoic deep-sea temperatures and global ice volumes from Mg/Ca in benthic foraminiferal calcite. *Science* 287, 269-272.
- Lee, Y.L., Hisada, K.I., 1999. Stable isotopic composition of pedogenic carbonates of the Early Cretaceous Shimonoseki Subgroup, western Honshu, Japan. *Paleogeogr. Paleoclimatol. Paleoecol.* 153, 127-138.
- Leier, A., Quade, J., DeCelles, P., Kapp, P., 2009. Stable isotopic results from paleosol carbonate in South Asia: Paleoenvironmental reconstructions and selective alteration. *Earth Planet. Sci. Lett.* 279, 242-254.
- Levin, N.E., 2013. Compilation of East Africa soil carbonate stable isotope data. Integrated Earth Data Applications. doi: 10.1594/IEDA/100221.
- Levin, N.E., 2015. Environment and climate of early human evolution. *Annual Review of Earth and Planetary Sciences* 43, 405-429.
- Levin, N.E., Brown, F.H., Behrensmeier, A.K., Bobe, R., Cerling, T.E., 2011. Paleosol carbonates from the Omo Group: Isotopic records of local and regional environmental change in East Africa. *Paleogeogr. Paleoclimatol. Paleoecol.* 307, 75-89.
- Li, X., Xu, W., Liu, W., Zhou, F., Wang, Y., Sun, Y., Liu, L., 2013. Climatic and environmental indications of carbon and oxygen isotopes from the Lower Cretaceous calcrete and lacustrine carbonates in Southeast and Northwest China. *Paleogeogr. Paleoclimatol. Paleoecol.* 385, 171-189.
- Licht, A., van Cappelle, M., Abels, H.A., Ladant, J.B., Trabucho-Alexandre, J., France-Lanord, C., Donnadieu, Y., Vandenberghe, J., Rigaudier, T., Lécuyer, Ch., Terry, Jr. D., Adriaens, R., Boura, A., Guo, Z., Aung Naing Soe, Quade, J., Dupont-Nivet, G., Jaeger, J.J., 2014. Asian monsoons in a late Eocene greenhouse world. *Nature* 513, 501-506. doi:10.1038/nature13704.

- Liu, B., Phillips, F.M., Campbell, A.R., 1996. Stable carbon and oxygen isotopes of pedogenic carbonates, Ajo Mountains, southern Arizona: implications for paleoenvironmental change. *Paleogeogr. Paleoclimatol. Paleoecol.* 124, 233-246.
- Liu-Zeng, J., Tapponnier, P., Gaudemer, Y., Ding, L., 2008. Quantifying landscape differences across the Tibetan plateau: Implications for topographic relief evolution. *Journal of Geophysical Research* 113, F04018.
- Macaulay, E.A., Sobel, E.R., Mikolaichuk, A., Wack, M., Gilder, S.A., Mulch, A., Fortuna, A.B., Hynek, S., Apayarov, F., 2016. The sedimentary record of the Issyk Kul basin, Kyrgyzstan: climatic and tectonic inferences. *Basin Res.* 28, 57-80.
- Mack, G.H., Cole, D.R., James, W.C., Girodano, T.H., Salvards, S.L., 1994. Stable oxygen and carbon isotopes of pedogenic carbonate as indicators of Plio-Pleistocene paleoclimate in the southern Rio Grande rift, south-central New Mexico. *American Journal of Sciences* 294, 621-640.
- Magaritz, M., Kaufman, A., Yaalon, D.H., 1981. Calcium carbonate nodules in soils: $^{18}\text{O}/^{16}\text{O}$ and $^{13}\text{C}/^{12}\text{C}$ ratios and ^{14}C contents. *Geoderma* 25, 157-172.
- Markwick, P.J., 2007. The paleogeographic and palaeoclimatic significance of climate proxies for data-model comparisons. In: Williams, M., Haywood, A.M., Gregory, J., Schmidt, D.N. (Eds.), *Deep-Time Perspectives on Climate Change: Marrying the Signal from Computer Models and Biological Proxies*. Geological Society Special Publication, 251-312.
- Markwick, P.J., Valdes, P.J., 2004. Palaeo-digital elevation models for use as boundary conditions in coupled ocean-atmosphere GCM experiments: a Maastrichtian (late Cretaceous) example. *Paleogeogr. Paleoclimatol. Paleoecol.* 213, 37-63.
- Mortazavi, M., Moussavi-Harami, R., Brenner, R.L., Mahboubi, A., Nadjafi, M., 2013. Stable isotope record in pedogenic carbonates in northeast Iran: Implications for Early

- Cretaceous (Berriasian – Barremian) paleovegetation and paleoatmospheric $P(\text{CO}_2)$ levels. *Geoderma* 211-212, 85-97.
- Neymark, L.A., Paces, J.B., Marshall, B.D., Peterman, Z.E., Whelan, J.F., 2005. Geochemical and C, O, Sr, and U-series isotopic evidence for the meteoric origin of calcrete at Solitario Wash, Crater Flat, Nevada, USA. *Environmental Geology* 48, 450-465.
- Nordt, L., Atchley, S., Dworkin, S.I., 2002. Paleosol barometer indicates extreme fluctuations in atmospheric CO_2 across the Cretaceous-Tertiary boundary. *Geology* 30, 703-706.
- Parcerisa, D., Gómez-Gras, D., Martín- Martín, J.D., 2006. Calcretes, oncolites, and lacustrine limestones in Upper Oligocene alluvial fans of the Montgat area (Catalan Coastal Ranges, Spain). In: Alonso-Zarza, A.M., Tanner, L.H., (Eds.), *Paleoenvironmental Record and Applications of Calcretes and Palustrine Carbonates*. Geological Society of America Special Paper, 416, 105-117.
- Pearson, P.N., Palmer, M.R., 2000. Atmospheric carbon dioxide concentrations over the past 60 million years. *Nature* 406, 695-699.
- Platt, N.H., 1989. Lacustrine carbonates and pedogenesis: sedimentology and origin of palustrine deposits from the Early Cretaceous Rupelo Formation, W Cameros Basin, N Spain. *Sedimentology* 36, 665-684.
- Plummer, T., Bishop, L.C., Ditchfield, P., Hicks, J., 1999. Research on Late Pliocene Oldowan sites at Kanjera South, Kenya. *Journal of Human Evolution* 36, 151-170.
- Poage, M.A., Chamberlain, C.P., 2001. Empirical relationships between elevation and the stable isotope composition of precipitation and surface waters: considerations for studies of paleoelevation change. *American Journal of Sciences* 901, 1-18.
- Potts, A.J., Midgley, J.J., Harris, C., 2009. Stable isotope and ^{14}C study of biogenic calcrete in a termite mound, Western Cape, South Africa, and its palaeoenvironmental significance. *Quaternary Research* 72, 258-264.

- Pucéat, E., Lécuyer, Ch., Sheppard, S.M.F., Dromart, G., Reboulet, S., Grandjean, P., 2003. Thermal evolution of Cretaceous Tethyan marine waters inferred from oxygen isotope composition of fish tooth enamels. *Paleoceanography* 18, 1029. doi:10.1029/2002PA000823.
- Quade, J., Cerling, T.E., 1995. Expansion of C4 grasses in the Late Miocene of northern Pakistan: evidence from stable isotopes of paleosols. *Paleogeogr. Paleoclimatol. Paleoecol.* 115, 91-116.
- Quade, J., Solounias, N., Cerling, T.E., 1994. Stable isotopic evidence from paleosol carbonates and fossil teeth in Greece for forest or woodlands over the past 11 Ma. *Paleogeogr. Paleoclimatol. Paleoecol.* 108, 41-53.
- Quade, J., Rech, J.A., Latorre, C., Betancourt, J.L., Gleason, E., Kalin, M.T.K., 2007. Soils at the hyperarid margin: The isotopic composition of soil carbonate from the Atacama Desert, Northern Chile. *Geochim. Cosmochim. Acta* 71, 3772-3795.
- Quinn, R.L., Lepre, C.J., Wright, J.D., Feibel, C.S., 2007. Paleogeographic variations of pedogenic carbonate $\delta^{13}\text{C}$ values from Koobi Fora, Kenya: implications for floral compositions of Plio-Pleistocene hominin environments. *Journal of Human Evolution* 53, 560-573.
- Retallack, G.J., Wynn, J.C., Fremd, T.J., 2004. Glacial-interglacial-scale paleoclimatic change without large ice sheets in the Oligocene of central Oregon. *Geology* 32(4), 297-300.
- Ringrose, S., Harris, C., Huntsman-Mapila, P., Vink, B.W., Diskins, S., Vanderpost, C., Matheson, W., 2009. Origins of strandline duricrust around the Makgadikgadi Pans (Botswana Kalahari) as deduced from their chemical and isotope composition. *Sediment. Geol.* 219, 262-279.
- Robinson, S.A., Andrews, J.E., Hesselbo, S.P., Radley, J.D., Dennis, P.F., Harding, I.C., Allen, P., 2002. Atmospheric $p\text{CO}_2$ and depositional environment from stable-isotope

- geochemistry of calcrete nodules (Barremian, Lower Cretaceous, Wealden Beds, England). *Journal of the Geological Society, London*, 159, 215-224.
- Rowe, P.J., Maher, B.A., 2000. 'Cold' stage formation of calcrete nodules in the Chinese Loess Plateau: evidence from U-series dating and stable isotope analysis. *Paleogeogr. Paleoclimatol. Paleoecol.* 157, 109-125.
- Salomons, W., Goudie, A., Mook, W.G., 1978. Isotopic composition of calcrete deposits from Europe, Africa and India. *Earth Surface Processes* 3, 43-57.
- Sandler, A., 2006. Estimates of atmospheric CO₂ levels during the mid-Turonian derived from stable isotope composition of paleosol calcite from Israel. In: Alonso-Zarza, A.M., Tanner, L.H. (Eds.), *Paleoenvironmental Record and Applications of Calcretes and Palustrine Carbonates*. Geological Society of America Special Paper, 416, 75-88.
- Schlesinger, W.H., 1985. The formation of calciche in soils of the Mojave Desert, California. *Geochim. Cosmochim. Acta* 49, 57-66.
- Schmid, S.M., Pfiffner, O.A., Froitzheim, N., Schönborn, G., Kissling, E., 1996. Geophysical-geological transect and tectonic evolution of the Swiss-Italian Alps. *Tectonics* 15(5), 1036-1064.
- Scotese, C.R., 2014a. Atlas of Early Cretaceous Paleogeographic Maps. PALEOMAP Atlas for ArcGIS, volume 2, The Cretaceous. DOI: 10.13140/2.1.4099.4560.
- Scotese, C.R., 2014b. Atlas of Late Cretaceous Paleogeographic Maps. PALEOMAP Atlas for ArcGIS, volume 2, The Cretaceous. DOI: 10.13140/2.1.4691.3284.
- Scotese, C.R., 2014c. Atlas of Paleogene Paleogeographic Maps (Molweide Projection). PALEOMAP Atlas for ArcGIS, volume 1, The Cenozoic. DOI: 10.13140/2.1.3417.6961.
- Scotese, C.R., 2014d. Atlas of Neogene Paleogeographic Maps (Molweide Projection). PALEOMAP Atlas for ArcGIS, volume 1, The Cenozoic. DOI: 10.13140/2.1.4151.3922.

- Scotese, C.R., Golonka, J., 1992. PALEOMAP Paleogeographic Atlas. PALEOMAP Progress Report #20, Dept. of Geology, University of Texas at Arlington. doi:10.13140/RG.2.1.1058.9202
- Sewall, J.O., van de Wal, R.S.W., van der Zwan, K., van Oosterhout, C., Dijkstra, H.A., Scotese, C.R., 2007. Climate model boundary conditions for four Cretaceous time slices. *Climate of the Past* 3, 647-657.
- Sheldon, N.D., 2018. Using carbon isotope equilibrium to screen pedogenic carbonate oxygen isotopes: Implications for paleoaltimetry and paleotectonic studies. *Geofluids* 2018, 5975801. doi:10.1155/2018/5975801
- Sheldon, N.D., Tabor, N.J., 2009. Quantitative paleoenvironmental and paleoclimatic reconstruction using paleosols. *Earth-Sci. Rev.* 93, 1-52.
- Sikes, N.E., Potts, R., Behrensmeyer, A.K., 1997. Pedogenic study of Pleistocene paleosols from the Olorgesailie Formation, southern Kenya rift. *Journal of Human Evolution* 37, 721-746.
- Sinha, A., Stott, L.D., 1994. New atmospheric $p\text{CO}_2$ estimates from paleosols during the late Paleocene/early Eocene global warming interval. *Glob. Planet. Change* 9, 297-307.
- Sinha, R., Tandon, S.K., Sanyal, P., Gibling, M.R., Stuben, D., Berner, Z., Ghazanfari, P., 2006. Calcretes from a Late Quaternary interfluvial in the Ganga Plains, India: Carbonate types and isotopic systems in a monsoonal setting. *Paleogeogr. Paleoclimatol. Paleoecol.* 242, 214-239.
- Srivastava, P., 2001. Paleoclimatic implications of pedogenic carbonates in Holocene soils of the Gangetic Plains, India. *Paleogeogr. Paleoclimatol. Paleoecol.* 171, 207-222.
- Strömberg, C.A.E., 2011. Evolution of grasses and grassland ecosystems. *Annu. Rev. Earth Planet. Sci.* 39, 517-544.

- Suguio, K., Berenholc, M., Salati, E., 1975. Composição química e isotópica dos calcários e ambiente de sedimentação da formação Bauru. *Boletim IG-USP* 6 (in Portuguese).
- Tandon, S.K., Sood, A., Andrews, J.E., Dennis, P.F., 1995. Palaeoenvironments of the dinosaur-bearing Lameta Beds (Maastrichtian), Narmada Valley, Central India. *Paleogeogr. Paleoclimatol. Paleoecol.* 117, 153-184.
- Tapponnier, P., Xu, Z.Q., Roger, F., Meyer, B., Arnaud, N., Wittlinger, G., Yang, J.S., 2001. Oblique stepwise rise and growth of the Tibet Plateau. *Science* 294, 1671-1677.
- Tippett, J.M., Kamp, P.J.J., 1995. Geomorphic evolution of the Southern Alps, New Zealand. *Earth Surf. Process. Landf.* 20, 177-192.
- Tipple, B.J., Meyers, S.R., Pagani, M., 2010. Carbon isotope ratio of Cenozoic CO₂: A comparative evaluation of available geochemical proxies. *Paleoceanography* 25, PA3202. doi: 10.1029/2009PA001851.
- Tripati, A., Darby, D., 2018. Evidence for ephemeral middle Eocene to early Oligocene Greenland glacial ice and pan-Arctic sea ice. *Nat. Commun.* 9, 1038. doi: 10.1038/s41467-018-03180-5.
- Vermeesch, P., 2012. On the visualisation of detrital age distributions. *Chem. Geol.* 312-313, 190-194.
- Wang, Y., Zheng, S.-H., 1989. Paleosol nodules as Pleistocene paleoclimatic indicators, Luochuan, P.R. China. *Paleogeogr. Paleoclimatol. Paleoecol.* 76, 39-44.
- Wang, Y., Deng, T., 2005. A 25 m.y. isotopic record of paleodiet and environmental change from fossil mammals and paleosols from the NE margin of the Tibetan Plateau. *Earth Planet. Sci. Lett.* 236, 322-338.
- Wernicke, B.P., Christiansen, R.L., England, P.C., Sonder, L.J., 1987. Tectonomagmatic evolution of Cenozoic extension in the North American Cordillera. In: Coward, M.P.,

- Dewey, J.F., Hancock, P.L. (Eds.), Continental Extensional Tectonics. Geological Society of London Special Publication, London, 28, 203-221.
- Wessel, P., Smith, W.H.F., 1991. Free software helps map and display data. EOS Transactions American Geophysical Union 72, 441, 445-446.
- Willett, S.D., Schlunegger, F., Picotti, V., 2006. Messinian climate change and erosional destruction of the Central European Alps. *Geology* 34(8), 613-616.
- Wynn, J.G., 2000. Paleosols, stable carbon isotopes, and paleoenvironmental interpretation of Kanapoi, Northern Kenya. *Journal of Human Evolution* 39, 411-432.
- Wynn, J.G., 2004. Influence of Plio-Pleistocene aridification on human evolution: Evidence from paleosols of the Turkana Basin, Kenya. *American Journal of Physical Anthropology* 123, 106-118.
- Wang, Y., Zheng, S.H., 1989. Paleosol nodules as Pleistocene paleoclimatic indicators, Luochuan, P.R. China. *Paleogeogr. Paleoclimatol. Paleoecol.* 76, 39-44.
- Wang, Y.D., Huang, C.M., Sun, B.N., Qian, C., Wu, J.Y., Lin, Z.C., 2014. Paleo-CO₂ variation trends and the Cretaceous greenhouse climate. *Earth-Sci. Rev.* 129, 136-147.
- Yonkee, W.A., Weil, A.B., 2015. Tectonic evolution of the Sevier and Laramide belts within the North American Cordillera orogenic system. *Earth-Sci. Rev.* 150, 531-593.
- Zachos, J., Pagani, M., Sloan, L., Thomas, E., Billups, K., 2001. Trends, rhythms, and aberrations in global climate 65 Ma to Present. *Science* 292, 686-693.
- Zeebe, R.E., 2001. Seawater pH and isotopic paleotemperatures of Cretaceous oceans. *Paleogeogr. Paleoclimatol. Paleoecol.* 170, 49-57.
- Ziegler, A.M., Rowley, D.B., Lottes, A.L., Sahagian, D.L., Hulver, M.L., Gierlowski, T.C., 1985. Paleogeographic interpretation: With an example from the Mid-Cretaceous. *Annu. Rev. Earth Planet. Sci.* 13, 385-428.

Figure captions:

Figure 1-A: Paleogeographic maps of the Lower Cretaceous (bottom) and Upper Cretaceous (top) from Scotese (2014a,b) showing the climatic zones (redrawn after Bouco et al., 2013). The location of the data used in this study is indicated by the encircled numbers. Note that for some of the continental blocks with rapid latitude variations such as India, the position of the data point on the map may not correspond to the paleo-latitude at the deposition time. Data source: Lower Cretaceous – 1- (Gregory et al., 1989); 2- (Mortazavi et al., 2013); 3, 4- (Huang et al., 2012); 5, 6- (Li et al., 2013); 7- (Lee and Hisada, 1999); 8- (Leier et al., 2009); 9- (Jolivet et al., 2018b); 10- (Platt, 1989); 11- (Robinson et al., 2002). Upper Cretaceous – 1-(Nordt et al., 2002); 2- (Erick and Glumac, 2014); 3- (Bojar et al., 2010); 4- (Tandon et al., 1995); 5–7- (Heilbronn et al., 2015; Jolivet et al., 2018); 8- (De Pelsmaeker et al., 2018); 9- (Leier et al., 2009); 10- (Suguio et al., 1975); 11- (Dworkin et al., 2005); 12- (Gao et al., 2015); 13- (Sand'ei, 2006); 14- (Ghosh et al., 1995).

Figure 1-B: Paleogeographic maps of the Paleocene (bottom, including all Paleogene data) and Middle Miocene (top, including all Neogene data) from Scotese (2014c,d) showing the climatic zones (redrawn after Bouco et al. (2013)). The location of the data used in this study is indicated by the encircled numbers. Data source: Paleogene – 1,- (Dworkin et al., 2005); 2- (Koch et al., 1995, 2003); 3- (Jolivet et al., 2018b); 4- (Macaulay et al., 2016); 5- (Hellwig et al., 2018); 6, 7- (Jolivet et al., 2018b); 8- (Bowen et al., 2005); 9- (Gao et al., 2015); 10- (Hoke et al., 2014); 11- (Alonso-Zarza and Arenas, 2004; Parcerisa et al., 2006); 12- (Garziona et al., 2008); 13- (Sinha and Stott, 1994); 14- (Caves et al., 2014); 15- (Clyde et al., 2001; Hyland and Sheldon, 2013); 16- (Retallack et al., 2004). Neogene: 1- (Fox and Koch, 2004); 2- (Fox and Koch, 2004; Fox et al., 2012); 3- (Mack et al., 1994); 4- (Ghosh et al., 2006); 5- (Latorre et al., 1997; Kleinert and Strecker, 2001); 6- (Jordan et al., 1996; Giambiagi, 1999; Irigoyen et al., 2000; Hoke et al., 2014); 7- (Alonso-Zarza and Arenas, 2004; Huerta et Armenteros, 2005; Hoke et al., 2014); 8- (Quade et al., 1994); 9- (Cerling et

al., 1988; Wynn, 2000, 2004; Cerling, 2011; Levin et al., 2011; Levin, 2013); 10- (Macaulay et al., 2016; Hellwig et al., 2018); 11- (Charreau et al., 2012); 12- (Heilbronn et al., 2015; Caves et al., 2017; Jolivet et al., 2018b); 13- (Caves et al., 2014); 14- (Kaakinen et al., 2006); 15- (Hoke et al., 2014); 16- (Quade and Cerling, 1995; Behrensmeyer et al., 2007); 17- (Aronson et al., 2008; Cerling, 2011); 18- (Cerling et al., 1991b; Kingston, 1992).

Figure 1-C: Present-day geographic map (top) simplified from Scotese (2014d) and climate map based on the Köppen-Geiger classification (bottom, drawn using the data from Kottek et al. (2006)) showing the complexity of the Quaternary climate. The location of the data used in this study is indicated by the encircled numbers. Data source: 1- (Neymark et al., 2005); 2- (Schlesinger, 1985; Liu et al., 1996); 3- (Mark et al., 1994; Deutz et al., 2001); 4- (Alomar, 2001; Fox and Koch, 2004; Fox et al., 2012); 5- (Kleinert and Strecker, 2001; Quade et al., 2007); 6, 7- (Sugio et al., 1975), 8- (Ringrose et al., 2009); 9- (Cerling and Hay, 1986; Sikes et al., 1997; Plummer et al., 1999); 10- (Cerling et al., 1988; Wynn et al., 2004; Quinn et al., 2007; Levin et al., 2011, 2015); 11-14- (Salomons et al., 1978); 15- (Salomons et al., 1978; Eren, 2011; Kaplan et al., 2013); 16- (Jolivet et al., 2018b); 17- (Rowe and Maher, 2000; Wang and Deng, 2005); 18- (Wang and Zheng, 1989; Wang and Deng, 2005); 19- (Alam et al., 1997); 20- (Srivastava, 2001; Sinha et al., 2006); 21- (Salomons et al., 1978, Andrews et al., 1998; Achyuthan, 2003; Dhir et al., 2010); 22- (Quade and Cerling, 1995; Achyuthan et al., 2012; Dar et al., 2015); 23- (Magaritz et al., 1981; Potts et al., 2009; Achyuthan et al., 2012); 24- (Aronson et al., 2008); 25- (Kingston et al., 1992; Garrett et al., 2015).

Figure 2: Kernel density estimation of $\delta^{18}\text{O}$ (left) and $\delta^{13}\text{C}$ (right) values for the Cretaceous to Quaternary carbonate-bearing paleosols (obtained using DensityPlotter, Vermeesch, 2012). N indicates the number of data for each histogram. The isotope values are reported using the conventional “ δ ” values using VSMOW as the standard for

oxygen (which implied recalculation of the delta value when it was reported against PeeDeeBelmenite in the original publication) and VPDB as the standard for carbon. The blue and green thick dotted lines indicate the trend of the mean value of the major peaks (indicated by a black cross) and the thin dotted lines the deviation from this trend in the Quaternary data or trends in secondary peaks for the Upper Cretaceous – Paleogene $\delta^{18}\text{O}$ data. Two histograms are shown for the $\delta^{18}\text{O}$ in the Lower Cretaceous, one (left) excluding the data from Gregory et al. (1989) that are clearly affected by a strong latitudinal effect. The deep-sea foraminifera $\delta^{18}\text{O}$ and $\delta^{13}\text{C}$ variation curves are from Zachos et al. (2001). The pictures to the left illustrate various types of paleosols: top, carbonate nodules and bottom, carbonate root cast (pictures M. Jolivet). The time-span of major events (glaciations, mountain uplifts and expansion of C4 flora) are reported, the increasing thickness of the grey envelope representing increases in mountain uplift rates. The references of the data and the data are reported in Supplementary Table S1, the geographic position of the studies are given on Fig. 1.

Figure 3: $\delta^{13}\text{C}$ versus $\delta^{18}\text{O}$ diagrams in plan view (left) and 3D (right) for the Paleogene, Neogene and Quaternary periods. *N* indicates the number of data. The probability density color contours highlight the major data clusters and were calculated from a kernel Gaussian density estimation using a Python (<https://www.python.org/>) script. Data clusters are labelled A to E. The dotted arrows in the Neogene plot indicate incipient effect of C4 plants on the $\delta^{13}\text{C}$ values and of topography on the $\delta^{18}\text{O}$ values. These effects are obvious in the Quaternary data (plain white arrows). The dotted arrow in the Quaternary plot indicate a trend probably combining C4 plants, topography and extreme aridity effects.

Figure 4: (A) Histograms of the distribution of global altitudes above sea level for the Lower Cretaceous, Upper Cretaceous and Quaternary. The Cretaceous topography has a $\sim 2.8^\circ$ latitude \times 2.8° longitude resolution (Sewall et al., 2007) and the Quaternary data have been interpolated on a 2° latitude \times 2° longitude using the USGS EROS Archive GTOPO30 database and the GMT software (Wessel and Smith, 1991). (B) Probability density curve of global altitudes above sea level at different periods showing the progressive increase elevation over 3000 m during the Miocene and Quaternary. Cretaceous and Quaternary data are as on Fig. 3A, Early Eocene data from Herold et al. (2014) and middle-Miocene data from Frigola et al. (2018).

Figure 5: Distribution of the mean isotopic values of each individual dataset as a function of the absolute paleo-latitude of the sampling site (the paleo-latitude is comprised between 0° (equator) and 90° (pole), regardless of the hemisphere). (a) $\delta^{18}\text{O}$ values for the Quaternary, (b) $\delta^{13}\text{C}$ values for the Quaternary. The dotted lines refer to specific latitude ranges detailed in the text.

Figure 6: $\delta^{18}\text{O}$ versus $\delta^{13}\text{C}$ diagrams of individual samples for various periods illustrating peculiar distributions. (a) Quaternary samples from Salomons et al. (1978) (red), Cerling and Hay (1986) (blue) and Potts et al. (2009) (green), showing positive correlations. (b) Neogene samples from Latorre et al. (1997) (red) showing positive correlation. (c) Quaternary samples from Wang and Zheng (1989) showing negative correlation (red). (d) Neogene samples from Charreau et al. (2012) showing a faint negative correlation. (e) Paleogene samples from Alonso-Zarza and Arenas (2004) showing a negative correlation and from Koch et al. (1995) showing a faint negative correlation (blue). (f) Quaternary samples from Alam et al. (1997) (blue) and Alomar (2001) (red) showing a wide spread in $\delta^{13}\text{C}$ values associated to a limited range of $\delta^{18}\text{O}$ values. (g) Neogene samples from

Behrensmeyer et al. (2007) showing a wide range of $\delta^{13}\text{C}$ values associated to a narrow spread in $\delta^{18}\text{O}$ values.

Supplementary Table S1: Isotopic data used in this study for the (A) Cretaceous, (B) Paleogene, (C) Neogene, (D) Quaternary. The isotope values are reported using the conventional “ δ ” values using VSMOW as the standard for oxygen (which implied recalculation of the delta value when it was reported against PeeDeeBelmenite in the original publication) and VPDB as the standard for carbon. ## indicate values that were not reported in the original publication or values identified by the authors as affected by diagenetic processes.

Declaration of interests

X The authors declare that they have no known competing financial interests or personal relationships that could have appeared to influence the work reported in this paper.

The authors declare the following financial interests/personal relationships which may be considered as potential competing interests.

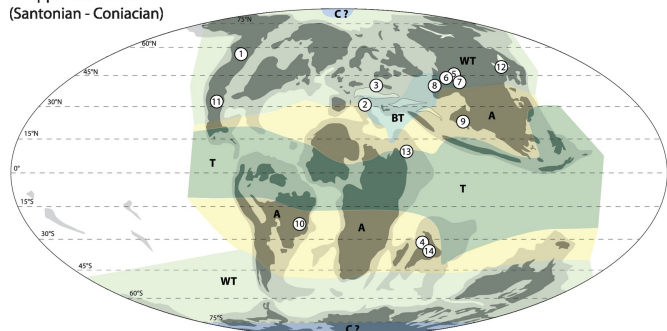
Global synthesis of O and C isotope composition of pedogenic carbonates

Cretaceous to Quaternary O and C isotope composition data in pedogenic carbonates

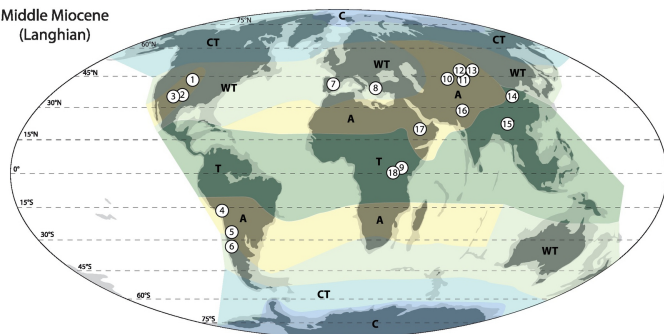
Continental global isotopic signals complementary to oceanic signals

Continent topography and associated enhanced aridity as major forcing parameter

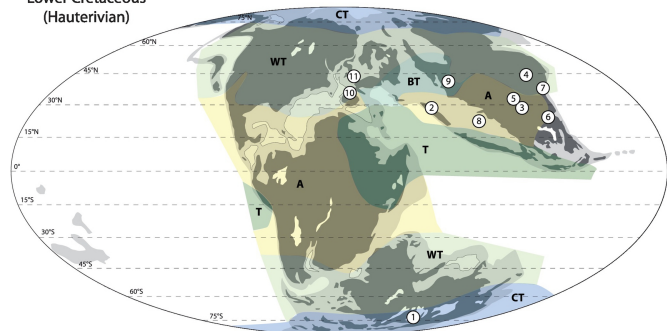
Upper Cretaceous
(Santonian - Coniacian)



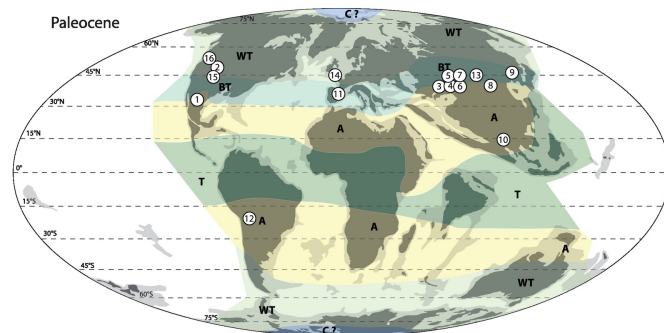
Middle Miocene
(Langhian)



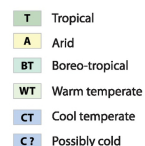
Lower Cretaceous
(Hauterivian)



Paleocene



Climate zones



Geography

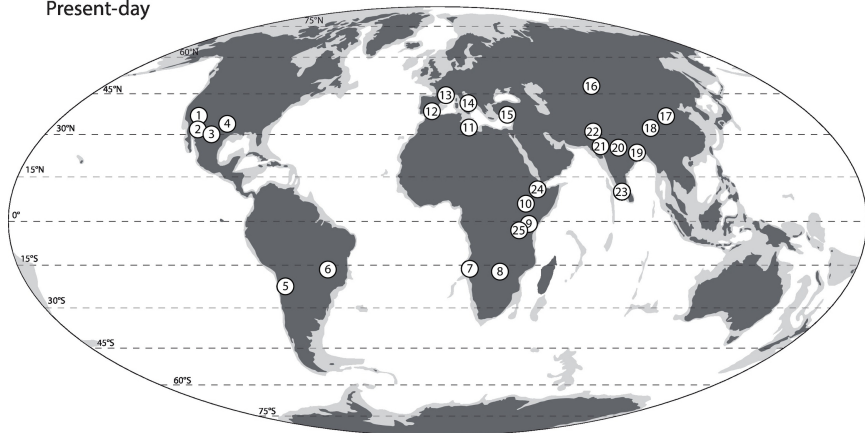


A

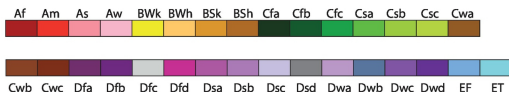
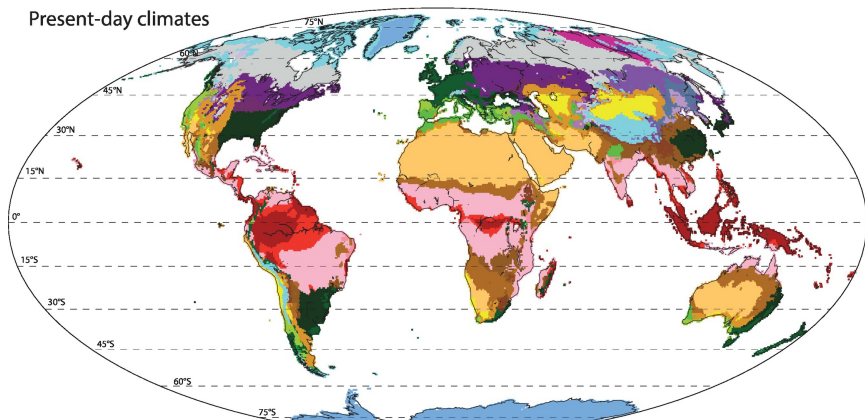
B

Figure 1A

Present-day



Present-day climates



Cwb Cwc Dfa Dfb Dfc Dfd Dsa Dsb Dsc Dsd Dwa Dwb Dwc Dwd EF ET

CLIMATES

A: equatorial
B: arid
C: warm temperate
D: snow
E: polar

PRECIPITATIONS

W: desert
S: steppe
f: fully humid
s: summer dry
w: winter dry
m: monsoonal

TEMPERATURE

h: hot
k: cold
a: hot summer
b: warm summer
c: cool summer
d: extremely continental
F: polar frost
T: polar tundra

Figure 1B

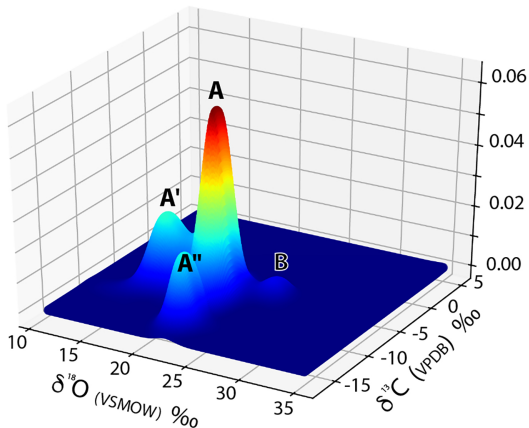
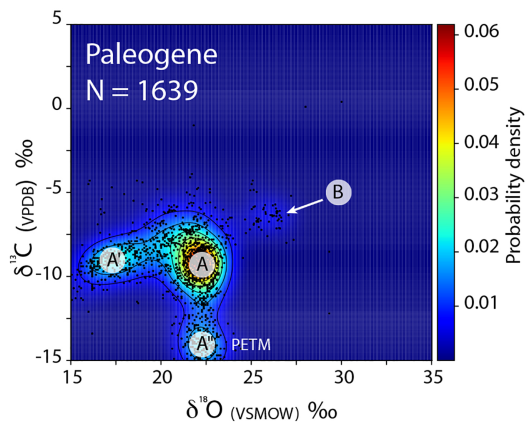
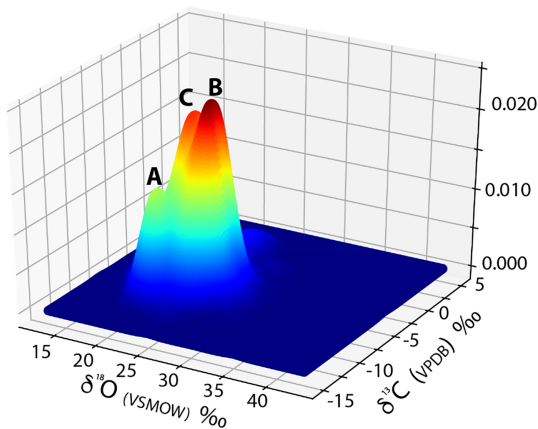
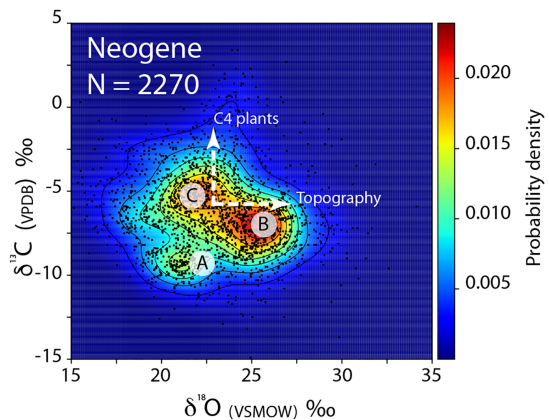
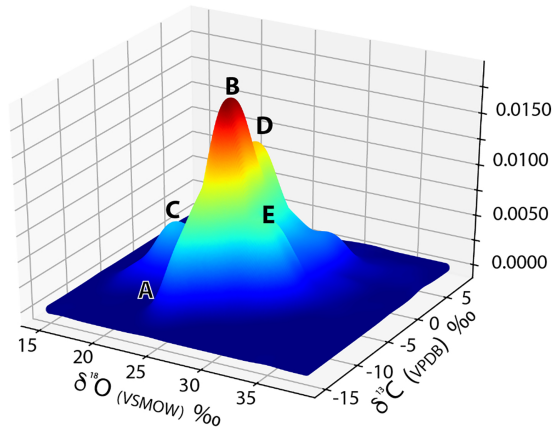
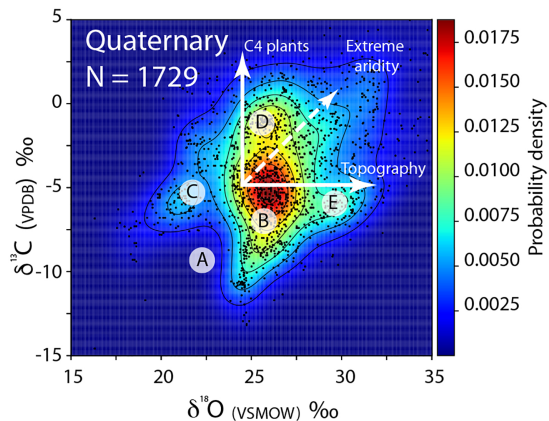


Figure 3

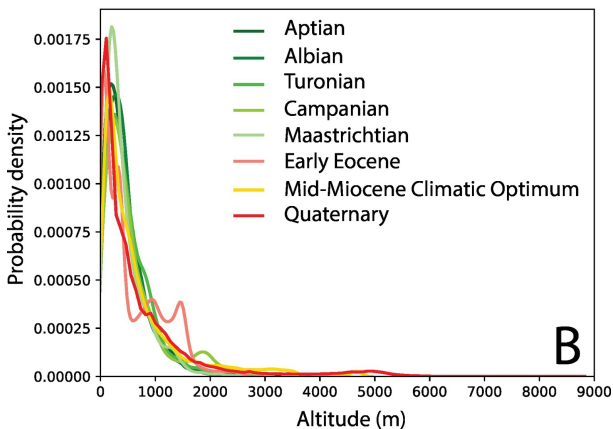
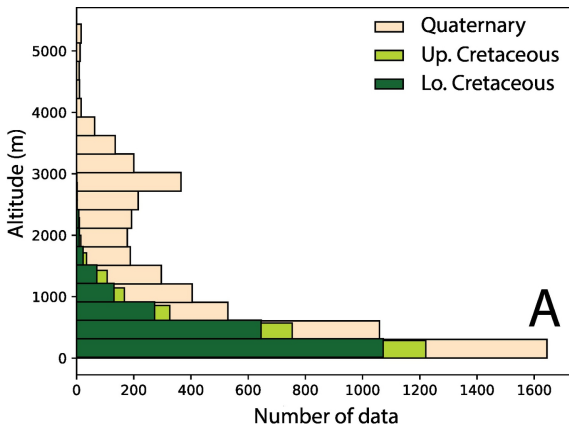


Figure 4

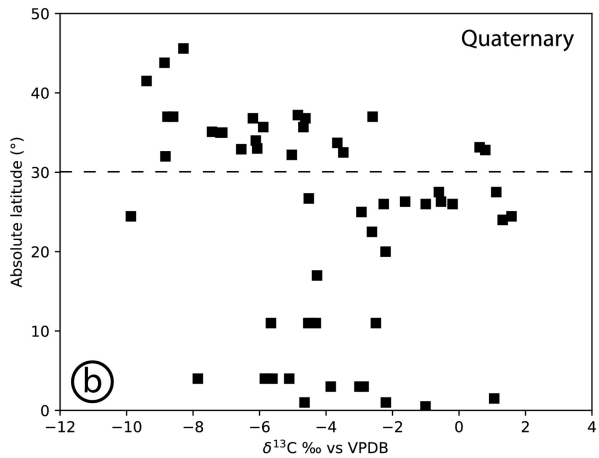
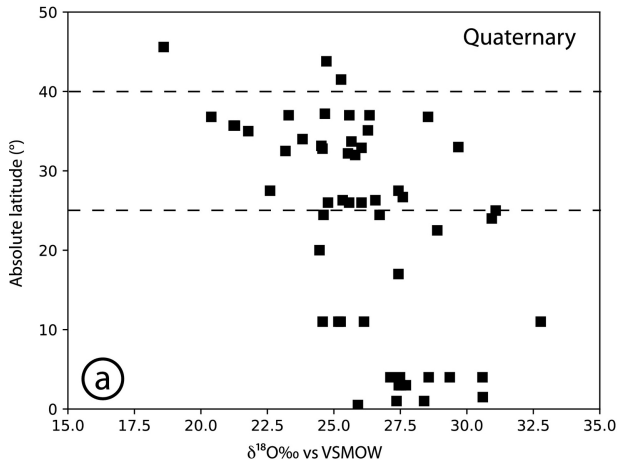


Figure 5

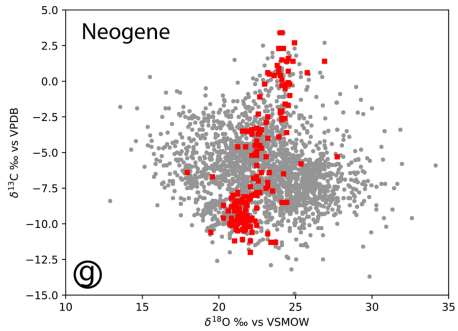
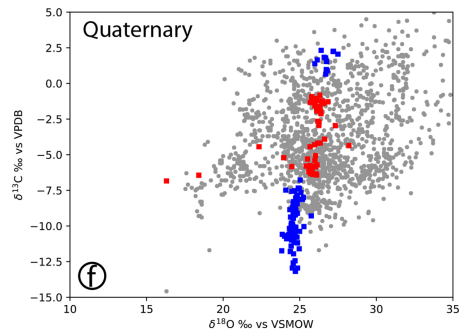
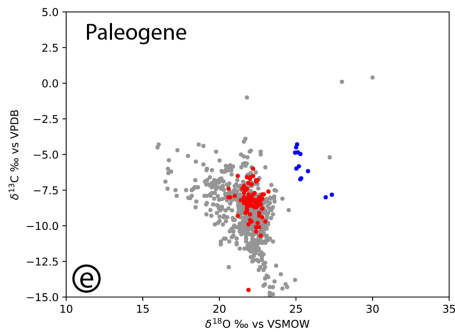
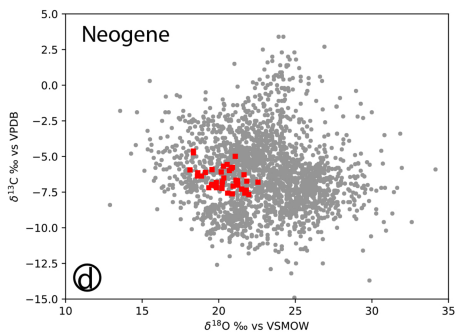
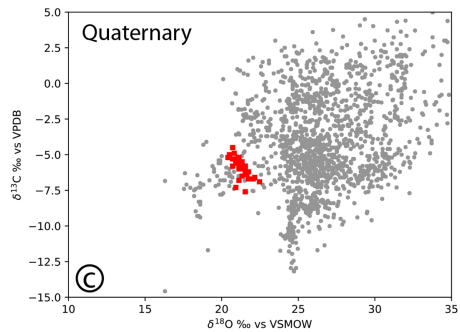
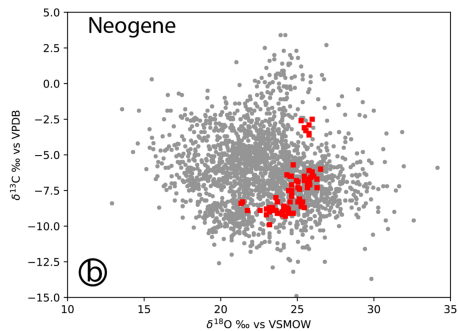
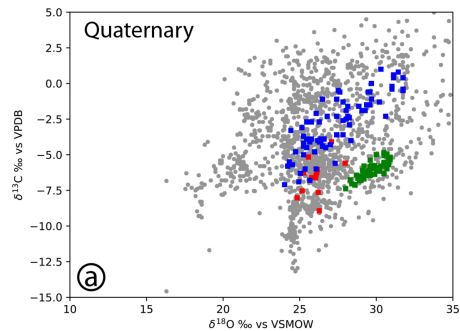


Figure 6